Journal of Molecular Graphics and Modelling 48 (2014) 96–104

Contents lists available at ScienceDirect

Journal of Molecular Graphics and Modelling

journal homepage: www.elsevier.com/locate/JMGM

Small molecule interaction with lipid bilayers: A molecular dynamics study of chlorhexidine

Brad Van Oosten[a,*], Drew Marquardt[a], Ivana Komljenović[b], Jeremy P. Bradshaw[c], Edward Sternin[a], Thad A. Harroun[a]

[a] Physics Department, Brock University, St. Catharines, Ontario L2S 3S1, Canada
[b] Physics Department, University of Guelph, Guelph, Ontario N1G 2W1, Canada
[c] College of Medicine and Veterinary Medicine, The University of Edinburgh, Edinburgh EH16 4SB, UK

ARTICLE INFO

Article history:
Received 7 October 2013
Received in revised form 2 December 2013
Accepted 17 December 2013
Available online 27 December 2013

Keywords:
Chlorhexidine
DMPC
Neutron diffraction
Slipids
NMR
GROMACS

ABSTRACT

Chlorhexidine (CHX) is an effective anti-bacterial agent whose mode of action is thought to be the disruption of the cell membrane. We tested the capability of the Slipids all atom force fields using data from neutron scattering and NMR experiments on the drug chlorhexidine in a 1,2-dimyrisoyl-3-*sn*-phosphatidylcholine (DMPC) membrane. Since it is not known what the charge of the CHX molecule is inside an apolar environment, a neutral, as well as a +1 and +2 charge model for the molecule were created and tested at several concentrations. This study shows that the location of CHX is minorly dependent on concentration, and dominantly reliant on the charge. The effect of adding CHX to DMPC is a thinning of the membrane, thus increasing the area per lipid.

1. Introduction

Molecular dynamics (MD) simulations, have become one of the powerful techniques to analyze the dynamic motion and gross structure of bio-membranes. MD simulations can reproduce the experimental environment of molecules in a computer and provide atomic-level information not detected in experiments. Over the last two years, more advanced force fields specific for lipid molecules have been developed, with experimental results in mind. Mainly, simulations are verified if they can properly reproduce NMR S_{CD} order parameters and form factors from neutron and X-ray scattering experiments [1–3].

Atomistic molecular dynamic simulations have tremendous utility for providing quantitative thermodynamic and mechanistic analysis of small molecule–lipid interactions. However, the typical time scale of such large simulations are below 200 ns, somewhat insufficient to detect larger molecule displacements or to obtain complete conformational sampling. Such simulations are made all the more difficult when looking for the effects of high concentration of the molecule, which only lengthens the computational time. This can preclude answering the typical key question of a membrane-active compound; where does a given solute reside within a bilayer and what factors govern its membrane binding or partitioning at equilibrium?

Coarse grained force fields have the advantage of having a simplified version of the modelled system which gives it the leverage of needing less computational time, leading to larger and longer simulations. However, coarse grain models have faired much worse in reproducing the thermodynamics of charged molecule–membrane interactions as a function of its protonation state, such as the case of the amino acid arginine important for ion channel modelling [4]. Although it is rare for a particular force field to be able to reproduce every known system, it is important to understand their limitations.

Biguanides are an important class of compounds, which resemble arginine, having multiple tautomers and protonation states. Their particular structure have shown to have extensive medical applications. Proguanil (an antimalarial agent) and Metformin (an antidiabetic compound) are biguanide derivatives, which are available as drugs [5,6]. Other important compounds in this series are phenformin, buformin, chlorophenylbiguanide, and chlorhexidine. Apart from the well-established antidiabetic and antimalarial effects, biguanide derivatives have been shown to exhibit antimicrobial, antiviral, and antiplaque effects and also have been known to influence gastric acid secretion [7–9].

We wanted to test the capability of one new lipid force field using data from neutron scattering to predict the partition location of the biguanide derivative drug chlorhexidine (CHX), shown in Fig. 1. This elongated flexible molecule presents an

* Corresponding author. Tel.: +1 9056885550x6174.
E-mail address: bv07ay@brocku.ca (B. Van Oosten).

1093-3263/$ – see front matter © 2013 Elsevier Inc. All rights reserved.
http://dx.doi.org/10.1016/j.jmgm.2013.12.007

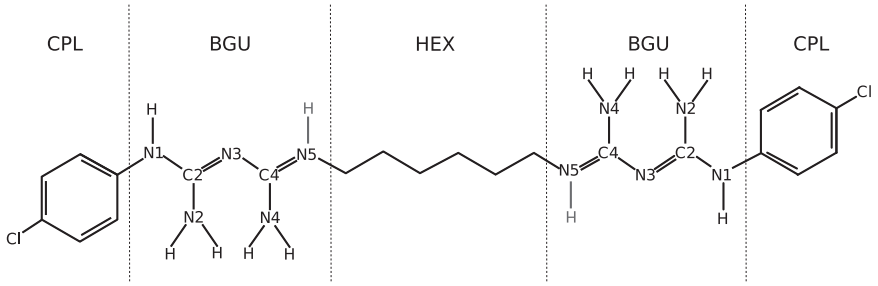

Fig. 1. Chlorhexidine representation with three groups; chlorophenol (CPL), biguanide (BGU) and hexane (HEX). Additional hydrogen atoms needed to create a CHX models with +1 and +2 charge are shown on the biguanide N5.

interesting biophysical modelling challenge; symmetrically composed of a (hydrophobic) hexane linker joining two (polar, hydrophilic) biguanides and (lipophilic) chlorophenol rings. We expect the free-energy competition between these subunits to determine the location of the CHX within a bilayer. We have previously experimentally established the location of the hexane of CHX in DMPC, at two high molar concentrations, using neutron diffraction in a manner that yields the time-averaged distribution within the bilayer.

The p*K*a in water of the similar compound, poly(hexamethylene-biguanide hydrochloride) (PHMB), was estimated to be around 13.5, meaning in aqueous solution at pH 7, PHMB will most likely exist in its +1 ionized form. Modelling studies have further showed that the most stable form of PHMB is one that has the +1 charge delocalized over the whole biguanide section, as would occur in the conjugated tautomer [10]. For CHX, the p*K*a of the singly ionized form was estimated to be 10.15, and doubly ionized at 9.55 [11]. The lower p*K*a indicates the biguanide in CHX is easier to deprotonate, but harder to protonate, than PHMB, becuase the chlorophenyl is less electron donating than an alkyl group [11].

However, the p*K*a of CHX or any biguanide has not been estimated when in an apolar environment. Only recently has it has been shown that the amino acid arginine may remain at least fractionally protonated even when in a low dielectric lipid hydrocarbon environment, although without some form of stabilization from additional negative amino acids or lipid molecules, there is significant disruption to the membrane structure as macroscopic quantities of water associate with the charge inside the normally hydrophobic region [12,13,4]. Since our system does not include such a stabilizing negative charge, nor do we see evidence of bulk water in the membrane, we began with the assumption that CHX is neutral, however we tested the +1 and +2 charge forms as well.

We wish to answer the following questions; can a CHX molecule find an equilibrium location in the bilayer (without prior knowledge) within a reasonable simulation time? What are the effects of adding additional charge to the CHX molecule? What are the effects of high concentration of CHX on the limited-sized simulation, and can those perturbations reproduce the experimental results?

2. Computational methods

We constructed an all-atom force field of chlorhexidine from the CHARMM36 force field [14–16] using well established parameters of certain amino acids [17]. Breaking the molecule into three sections as shown in Fig. 1; the chlorophenol ring, biguanide and hexane, for which we selected the bond lengths, angles and torsions from Tyr, Arg, and Lys respectively.

Partial charges were calculated usung GAUSSIAN software [18] and methods used for refining all-atom force feilds [1]. The partial charges taken from the amino acids Tyr, Arg and Lys to create a first approximation model of chlorhexidine. This model was simulated in a box of methanol to produce a dielectric constant similar to that of the headgroup region of lipids where the molecule has been experimentally observed to reside [19]. The simulation was run for 1 ns, where 500 different snapshots of the molecule were taken 2 ps apart. For each conformation, atomic charges were computed with the DFT method using B3LYP exchange-correlation functional with the cc-pVTZ basis set. The partial charges of each atom were then averaged over the 500 snapshots to achieve a partial charge that takes into account the distribution of conformations during a simulation in a lipid system. The newly obtained charges were then used in the structure of chlorhexidine for further simulations.

Additional information is required for an accurate representation of the bond structure and chemistry of the biguanide sections. Amide bond resonance has been a topic of much study, including theoretical studies of guanides and biguanides. [20–22]. The general consensus from these quantum chemistry calculations is that the configuration of the most stable neutral tautomer is characterized by conjugative interaction of the π-bonds, leading to alternating single and double bonds along the backbone, and therefore no hydrogen atom on the central nitrogen atom N3 (See Fig. 1). This means two hydrogen attached to each of the N2 and N4 nitrogen, and the final hydrogen then rests on either N1 or N5. Placing it on N1 fixes the double bonds to be between C2-N3 and C4-N5. The alternative tautomer would likely be entirely equivalent. A +1 charged CHX involves placing an additional hydrogen on the N5 of just one of the ends of the molecule, and a +2 charge would place a hydrogen on the N5 of both biguanide sections.

An initial 3D structure of the neutral, +1, and +2 charged chemical schematics shown in Fig. 1 was constructed using the OpenBabel [23,24] from the appropriate SMILES representation, and then refined by hand in the software Avogadro [25]. The structure was then optimized using self-consistent field theory with closed-shell restricted Hartree–Fock (RHF) wavefunctions to the level of 6-31G* with the software NWChem [26]. The final bond lengths did not differ by more than 0.05 nm from those of the CHARMM36 force field. The final topology of CHX can be found in the supplementary information.

The topology of 1,2-dimyristoyl-3-*sn*-phosphatidylcholine (DMPC) was obtained from the Stockholm lipids website [1,2]. Initial coordinates of a 128-lipid DMPC bilayer in an $8 \times 8 \times 2$ configuration were obtained from CHARMM-GUI [27] with 30 TIP3P water molecules per lipid. The system was checked for correctness by running a pure bilayer simulation for 100 ns at 303 K and 323 K. Such lipid force fields are continually being validated and refined, and reproduce the essential characteristics of pure lipid bilayers accurately [28,29].

All simulations were performed using the GROMACS simulation software (version 4.6.1) [30] for 100 ns at 323 K followed by another 100 ns at 309 K, under periodic boundary conditions in a simple orthorhombic box. Systems containing charged CHX models were neutralized by adding Cl ions into the water in order to achieve a system with zero net charge. The temperature of the

system was maintained by independently coupling the lipids, solvent, and CHX to an external temperature bath with a coupling constant of 1.0 ps using a Nose-Hoover thermostat. The pressure was kept at 1.013 bar in the lateral and normal directions independently by weakly coupling to a semi-isotropic pressure bath, using an isothermal compressibility of 4.5×10^{-5} bar^{-1} and a coupling constant of 10 ps.

A 2-fs time step with a Leap-Frog integrator was used. The Verlet list group scheme was used to for its optimal usage with GPUs for an increased simulation speed-up. The Verlet list scheme keeps a buffered list with exact cut-offs which are updated every 20 steps. Both the Coulomb and LJ potentials are shifted to zero with an exact cut-off value of 1.4 nm.

3. Results

Initially, two systems were constructed where a single neutral CHX was added to the simulation box, either outside the membrane in the water, or in the middle of the bilayer among the lipid terminal methyls. The latter case involves "exploding" the bilayer by artificially scaling the distance between lipids in each direction until sufficient room is made for the CHX, then slowly iterate between rescaling and energy minimization until the bilayer is reassembled. No lipids were removed. Solvating with water, and equilibration followed, as described above.

Fig. 2 shows the the center of mass distribution for the hexane region of CHX during the subsequent 100 ns NPT runs at 323 K, for both simulations. In the course of reassembling the bilayer, the CHX starting from the centre was no longer quite in the center, but starting a location ~ 0.2 nm higher, it quickly adopts a new location at ~1 nm where it remains for the remainder of the simulation. The CHX started from the water however, continues to oscillate with nearly 1 nm amplitude in the water until ~ 10 ns, at which point it begins to interact more strongly with the lipids. Just before ~ 15 ns, it rapidly inserts into the bilayer, and the two systems become indistinguishable in structure and energy. CHX is clearly highly mobile in water phase, but reaches an equilibrium location in the membrane interior that remains for the rest of the 100 ns simulation.

It is likely that at the end, both simulations reflect the free-energy minimum location of CHX in DMPC bilayers, and it is unlikely they will eventually come out of the bilayer with continuation of the simulation past 100 ns. Fig. 2 also shows the system potential energy of the water-born CHX during the run. The potential energy change upon CHX insertion cannot be seen visually, however, following the methods of Schiferl and Wallace, level changes can be tested for statistical significance via sampling two regions of interest in the energy [31]. Testing whether the mean energy from 1 to 10.0 ns (from 10,000 data points), is different from the mean from 80 to 100 ns (from 20,000 data points) shows statistical significance ($p < 0.001$, Cohen's $d = 0.19$), whereas two different sets of data drawn from 1 to 4 ns and 4 to 8 ns are not statistically different ($p > 0.2$). Thus the CHX insertion can be seen from the noisy energy data as a small, but highly significant effect.

Confident an equilibrium position for CHX exists, and that a 100 ns time frame was sufficient, we constructed simulations of 4 and 12 CHX within a 128 lipid DMPC bilayer, where all the CHX begin in the water layer, equally divided on opposite sides of the bilayer. In order to facilitate the insertion of such a large number of molecules, the simulations were initially run for 100 ns at 323 K, before an additional 100 ns simulation was run at 303 K. Fig. 3 shows the individual insertion of 12 CHX, beginning with four around 5 ns, and ending with the last insertion at 35 ns. Data

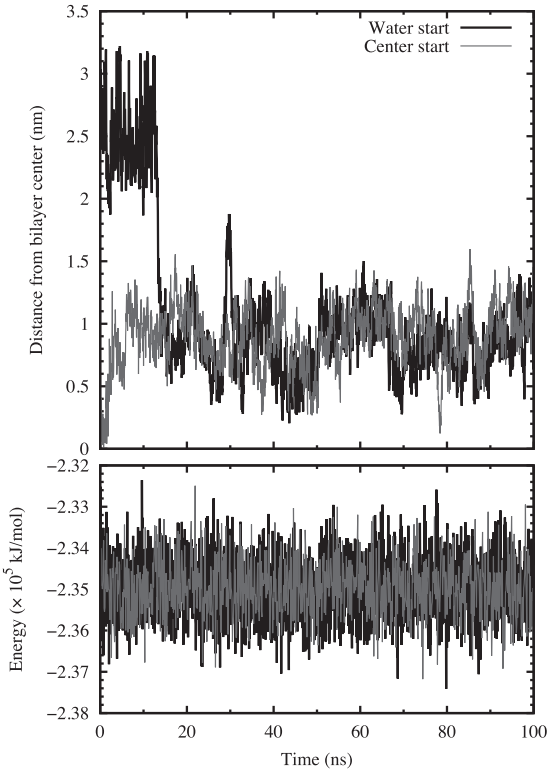

Fig. 2. Comparison of the distance between the center of mass of the CHX HEX and the lipid terminal methyls (upper frame) and the system potential energy (lower frame) for chlorhexidine simulations started from outside the bilayer in the water (black) or the center of the membrane (red). Both simulations are indistinguishable at the end.

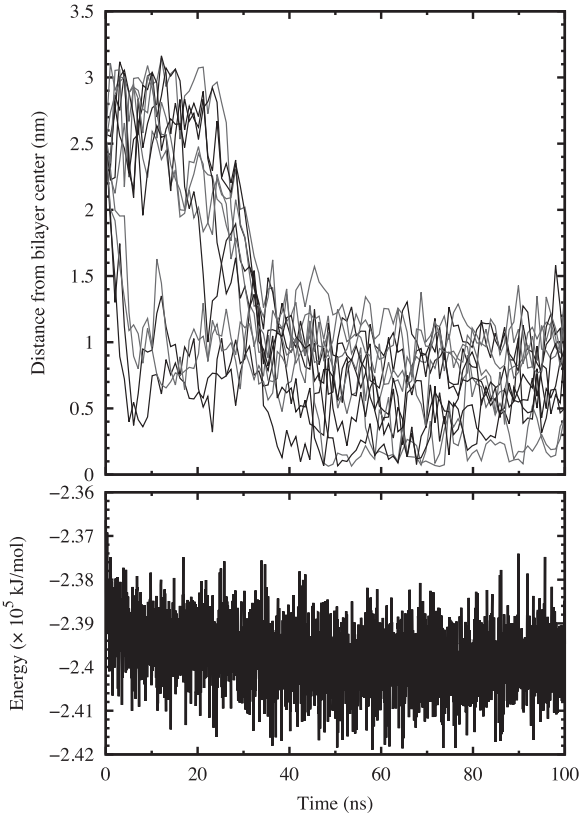

Fig. 3. (Upper panel) Distance between the center of mass of all twelve neutral CHX HEX and the lipid terminal methyls, showing insertion of each at various times. The traces have been smoothed and some have been colored for clarity. (Lower panel) The system potential energy.

Table 1
Statistical analysis of the system energy.

	Insertion energy (kJ/mol/CHX)	12 CHX drift in energy (kJ/mol/100 ns)
Neutral CHX	50–60	627
+1 charge CHX	30–40	378
+2 Charge CHX	25–30	182

shown are spline fits to reduce noise and provide clarity of the trend. No appreciable aggregation of the CHX was seen in the simulation, although one could argue that after the first 4 molecules inserted, the others very quickly followed suit as a group. The drop in system energy is more clear in Fig. 3, and the energy of insertion was calculated to be 706 ± 101 kJ/mol. This is less on a per molecule basis than the single CHX simulation, and probably a reflection of some inter-CHX association, as well as the partial insertion of 1-3 CHX at the end of the equilibration period and beginning of the simulation. At the end of the simulation the location of the twelve CHX seem to be randomly distributed between the center of the bilayer and 1.3 nm. We will show below that the full time- and system-averaged distribution of the CHX is more localized than Fig. 3 would suggest. Simulations with a +1 and +2 charged CHX show qualitatively similar behaviour to the neutral case; insertion in the first 10–40 ns, with a concomitant decrease in system energy.

While not every case of a single CHX insertion passed statistical significance, every 323 K insertion of 4 and 12 CHX did. However, the size of the effect was small, and in Table 1 we present the spread of values of the energy of insertion calculated from a 4 ns range average at the simulation beginning versus the end. As expected, the energy of insertion of the more polar +2 charged CHX was less than +1 charged and neutral CHX, since the neutral CHX will sequester itself further from the water into the hydrocarbons than either the charged species. Below, we will confirm this.

Since the 303 K simulations followed on from the 323 K runs, we do not expect any change of state in the course of the run, and in fact, none of the very small changes in the energy level for the 1 or 4 CHX runs passed any statistical test for significance, indicating stable equilibrium and no energy drift over 100 ns. However, the 12 CHX at 303 K simulations showed a small but significant drift in energy, also shown in Table 1. At this high concentration and lower temperature, true equilibration may take longer than 100 ns. In this case, as we will see below, since the neutral CHX are more free to explore a greater region of the bilayer center, the energy drift is larger than the +2 charged CHX, which has established a much narrower distribution in the bilayer, indicative of less mobility. In either case, we do not expect any changes to our structural analysis below, as these energy drifts are so small, they can only be detected with statistical analysis.

The principle difference between the 1, 4, and 12 CHX simulations comes in the final insertion depth of CHX. To measure this, we compare our results with the neutron diffraction data from Komljenovic et al., where we determined the depth of deuterium labelled CHX hexane in DMPC at concentrations of 1:3 and 1:10 CHX:DMPC using crystallographic methods and isotopic labelling [19]. The simulation results are shown in Fig. 4 as the time- and sample-averaged location of the CHX hexane hydrogen across the bilayer, in principle, a direct correspondence to the previous neutron diffraction experiments. In both the neutral or charged cases, there is a narrow, 0.6–0.8 nm width Gaussian-shaped mass distribution of CHX in the bilayer.

For each CHX simulated, there is a small concentration dependence in the location of the CHX, and a more significant dependence on CHX charge. For the case of neutral CHX, the final position of the hexane is 0.8 nm from the bilayer centre, although in the crowded environment of 12:128 CHX:DMPC, the extra CHX molecules find

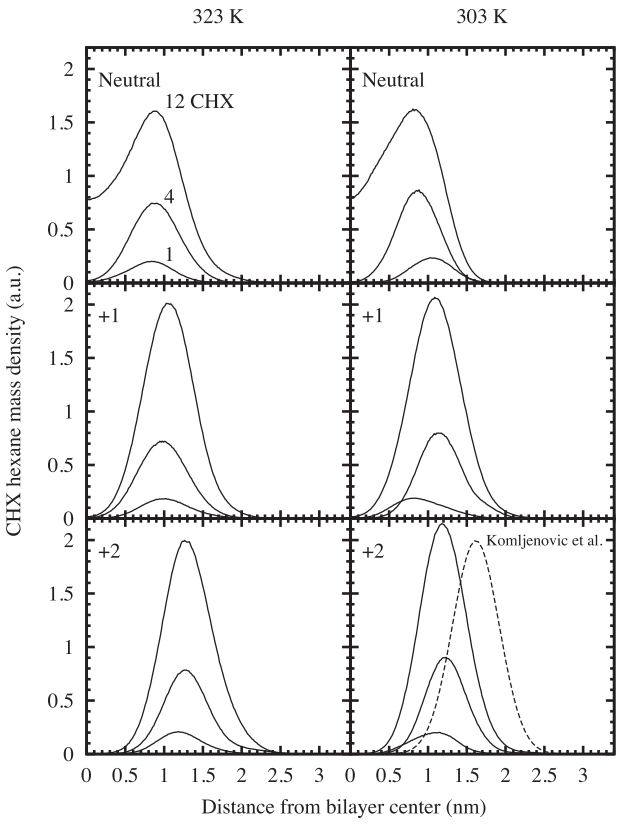

Fig. 4. HEX distributions for each concentration (1:128, 4:128, 12:128 CHX:DMPC) of neutral (upper frame), +1 charged (center frame) and +2 charged CHX (lower frame) at both 323K and 303K. The HEX distribution determined by neutron scattering is added to the bottom right frame for comparison [19].

extra room in the center of the bilayer. Only at 303 K do we see the effect of reduced lipid chain motion forcing the CHX equilibrium location toward the bilayer center with increasing concentration. For the +1 and +2 charged cases, the charge pulls the CHX closer to the hydrophobic/hydrophillic interface, to a higher location of 1.1 and 1.3 nm respectively. At high concentrations, CHX is no longer crowded to the center of the bilayer, but rather increasing the amount of CHX moves them further out, towards the aqueous interface.

However, none of the simulations agree with the experimentally determined mass density of the same hexane deuterium label shown as the dashed line in the lower panel of Fig. 4. In that case, we measured the hexane to be much higher in the membrane, at 1.6 nm from the bilayer center. The reason appears to be differences in the bilayer structure between simulation and experiment, and notably, the much deeper penetration of water into the simulated membrane. This has the effect of lowering the water interface, to which the CHX is clearly attracted, deeper into the bilayer.

Fig. 5 shows the neutron scattering length density for the 1 and 12 CHX simulated systems, separated into bilayer and water components. Only half the bilayer is shown, starting from the central lipid methyls shifted to be at 0 nm, and extending to the water layer at the right. Neutron scattering length density is analogous to the more commonly measured electron density, with slight differences in the interpretation of Fig. 5. The dip in signal in the bilayer center is due to the negative neutron scattering length of the CH_3 hydrogen. The peak around 1.2-1.5 nm is not the high number of electrons of the phosphate, but rather is representative of the low density of hydrogen around the glycerol–ester backbone. [32]

Overall, there is little difference in the curve shapes between the simulations. The extra mass of the higher number of CHX can

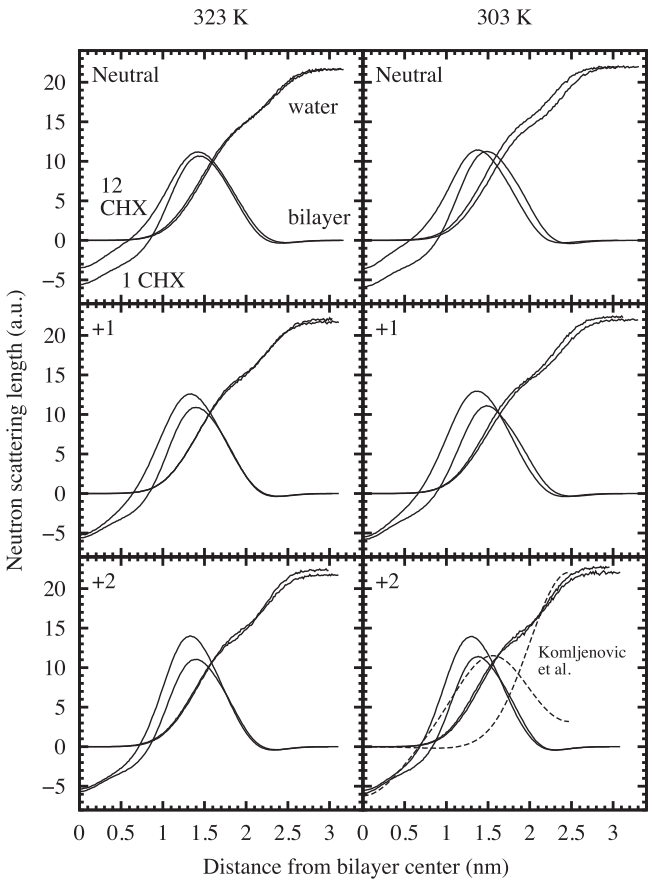

Fig. 5. Comparison of the neutron scattering length density of CHX:DMPC bilayers or the extra-bilayer water profiles for the 1:128 and 12:128 CHX:DMPC concentrations. The dotted line in the bottom right frame represents the results from neutron scattering from Komljenovic et al., at 1:10 CHX:DMPC [19].

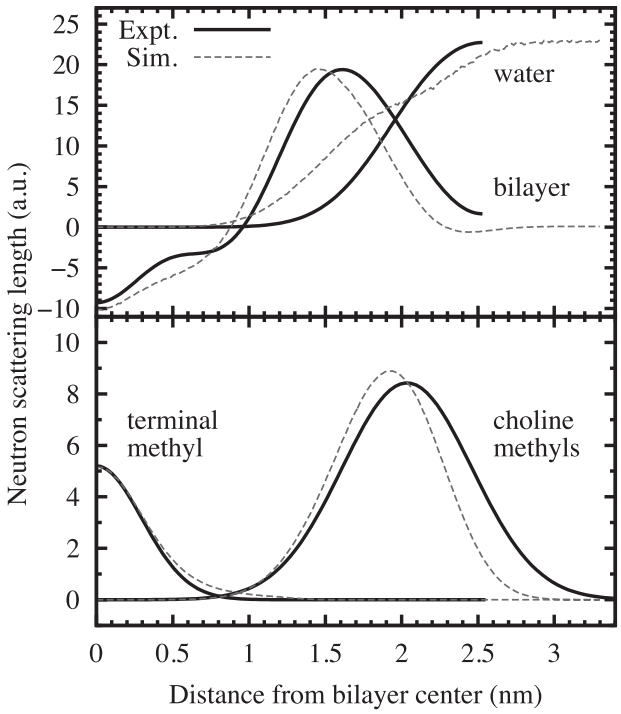

Fig. 6. Comparison of the experimental (solid) and simulated (dashed) neutron scattering length density of either the bilayer or external water penetration (upper frame) as well as the neutron scattering length density (mass distribution) of the terminal and choline methyl hydrogen (lower frame).

be seen in the curves of the 12 CHX over the 1 CHX. Most importantly, however, the bilayer experiences 0.3 nm thinning with the +2 charge over the neutral simulation. As the CHX moves from the bilayer center to the surface, the bilayer thins in response. In all cases the water layer shape remains roughly the same, showing two layers of hydration. The first layer penetrates into the bilayer to the level of the phosphates, and are the direct hydration of the choline headgroups (6–10 waters per lipid), and the remaining layer is bulk water.

We also include the experimental data of Komljenovic et al. in the lower panel of Fig. 5 for the concentration of 1:10 CHX:DMPC at 309 K. [19] The bilayer data is obtained with a composition of 8% ^2H_2O, which renders the water "invisible" to neutrons and the resulting data is entirely due to scattering from only the lipids and CHX, directly comparable to the simulation data. We see that the structure of the bilayer interior is well simulated, however, the headgroups are broader and the bilayer is thicker. Repeating the experiment with higher concentration of ^2H_2O, and subtracting the results, gives the water profile shown in Fig. 5. The experiment firmly rules out water penetrating deeply into the headgroups, effectively moving the hydrophilic/hydrophobic interface much higher in the bilayer, where the CHX follows suit.

To see this result more clearly, we compare simulations of pure DMPC without CHX to previously unpublished data on the distribution of water and two key components of the lipid bilayer; (1) the hydrogen of the *sn*-1 acyl chain terminal methyl and (2) the nine hydrogen of the choline methyl groups. (Experimental methods can be found in supplementary information.) Our simulations of pure DMPC bilayers reproduce the published results without issue, and the key parameters of the simulation, the area per lipid and bilayer thickness, are provided in Table 2 [1,2]. Fig. 6 shows the distribution of these lipid groups (lower panel) and the overall bilayer and water (upper panel). We see that the distribution of terminal methyls are reproduced very well. The overall distribution of the choline methyl groups is not as well represented, the experiment indicating a 0.2 nm thicker membrane and slightly wider distribution. The same experimentally determined 0.2 nm thickness difference is seen also seen in the overall bilayer structure. Although the plateau in the acyl chain region is not as well defined in the simulation, the overall impression is a remarkable comparison between simulation and experiment on bilayer structure.

However, the experiment is unambiguous on the exclusion of inter-bilayer water from the phosphate region and below. If we define the hydrophobic/hydrophilic interface to be the half-max position of the water distribution, the experiment indicates that to be 1.9 nm, and the simulation at 1.6 nm. There are several important differences in the two systems that prevent a direct and fair comparison; lower hydration in the neutron diffraction, and poor experimental resolution in the validation of the simulation parameters, that may contribute to this discrepancy, and which we will further review in the discussion.

Fig. 7 shows the S_{CD} order parameters of averaged over both $sn-1$ and $sn-2$ tails for each CHX model. The simulation results slightly underestimates the experimental values for pure DMPC (upper frame) performed at 308 K, which is known property of the Slipids force field [1]. The splitting of order parameter for the second carbon in the *sn*-2 chain is not well reproduced, however, the overall underestimation of S_{CD} indicates the lipids are more, rather than less, disordered and all in the L_α phase.

The effect of CHX on the order parameter of the lipid chains was negligible at the lower concentrations and only showed deviation from the pure DMPC system at the highest 12:128 concentrations. The change in disorder of the acyl chains was also dependent on the charge of the CHX. The neutral CHX exhibits an ordering effect

Table 2
Simulated membrane parameters.

		323 K		303 K	
		Area/lipid (Å^2)	Thickness (Å)	Area/lipid (Å^2)	Thickness (Å)
	Pure DMPC	62.44(2)	28.2(2)	61.16(2)	29.1(2)
	1:128	63.50(1)	29.0(2)	61.55(1)	30.0(2)
Neutral	4:128	64.71(1)	29.2(2)	62.38(1)	29.0(2)
	12:128	66.38(1)	29.6(2)	64.38(1)	28.6(2)
	1:128	63.55(1)	27.8(2)	61.07(1)	29.8(2)
+1 Charge	4:128	64.62(1)	28.4(2)	62.48(1)	28.4(2)
	12:128	67.54(1)	28.4(2)	65.37(1)	28.8(2)
	1:128	63.34(1)	28.2(2)	61.48(1)	27.8(2)
+2 Charge	4:128	64.52(1)	28.4(2)	62.40(1)	29.0(2)
	12:128	68.00(3)	27.4(2)	66.18(1)	27.2(2)

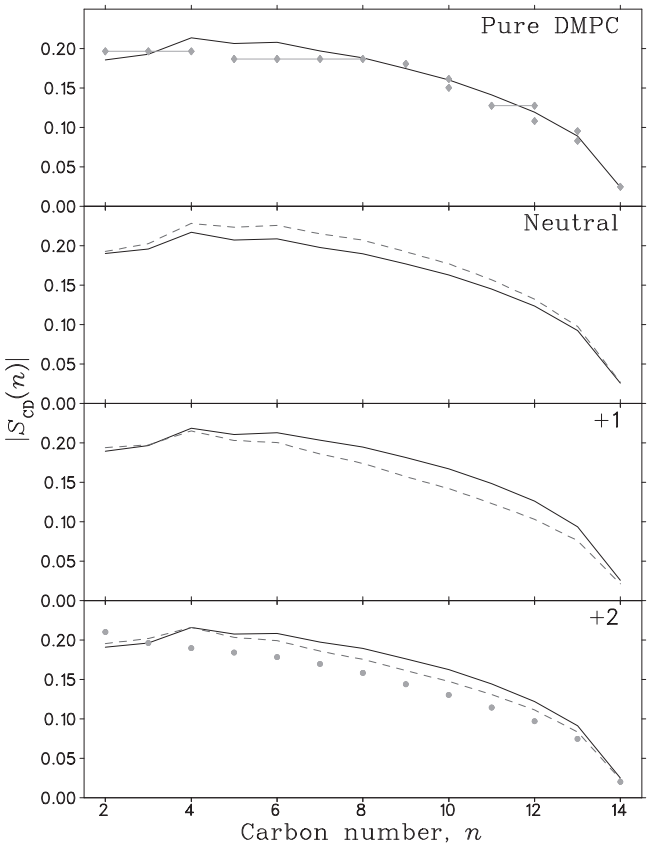

Fig. 7. DMPC simulated lipid deuterium order parameters of 1:128 (solid) and 12:128 (dashed) CHX:DMPC concentrations at 308 K. Experimental data, also at 308 K, are also shown for pure DMPC (diamonds, upper frame) and at 1:10 CHX:DMPC concentration (circles, lower frame).

on the DMPC chains, which is in complete contrast to the charged models which lower the chain order. The difference in the effect between the +1 and +2 charge are minimal with the +2 charge effecting the chains at a slightly higher position than the +1 charge CHX, due to its higher equilibrium position.

In the lower panel of Fig. 7, we show previously unpublished experimental NMR lipid order parameters for 10:1 CHX in DMPC at 308 K. (NMR experimental methods can be found in supplementary information.) The simulations achieve very good agreement in magnitude and shape of the curve. The simulations slightly overstate the values of S_{CD} for carbons 4 through 11.

The hydrogen atoms in the biguanide section of CHX act as hydrogen bond donors with the ability to establish hydrogen bonds with the oxygen atoms of the lipid molecules. The lifetime of these

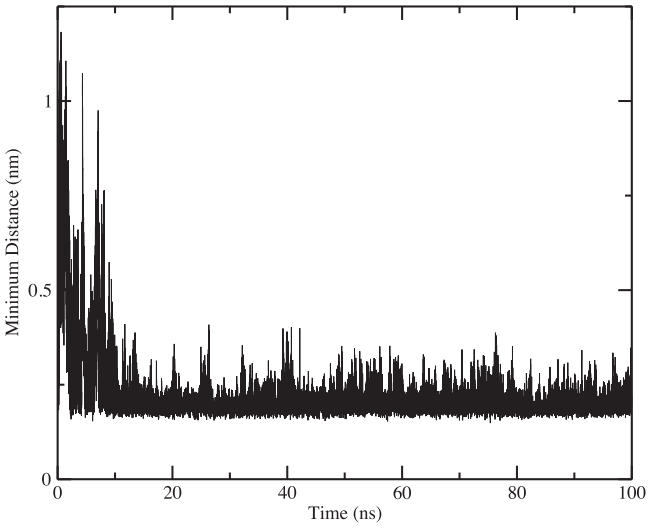

Fig. 8. Minimum distance between the additional hydrogen of the biguanide (BGU) group and the lipid phosphate oxygen for the +1 charged CHX at 323 K.

hydrogen bonds has been observed to be on the order of the length of the simulations. Fig. 8 shows the minimum distance between the hydrogen on the BGU section of the +1 CHX and the lipid phosphate oxygen at 323 K. After the insertion of the molecule, the hydrogen atom stays at a close ~0.2 nm from the lipid oxygen atom, with small jumps where it switches from lipid to lipid.

Table 3 shows the average number of hydrogen bonds made during the last 50 ns of each simulation, after all of the CHX molecules have inserted into the bilayer. The neutral CHX makes on average 1.5 hydrogen bonds per molecule once inserted into the membrane. The charged CHX models have additional hydrogen atoms, which allow for additional bonds to be made with the lipids. The +1 charge

Table 3
Number of hydrogen bonds between CHX biguanide and lipid phosphate oxygen.

		323 K		303 K	
		H-bonds	Per CHX	H-bonds	Per CHX
	1:128	1.16	1.16	1.50	1.50
Neutral	4:128	2.25	1.39	5.56	1.39
	12:128	3.22	0.96	13.03	1.09
	1:128	2.44	2.44	2.44	2.44
+1 Charge	4:128	9.54	2.39	10.87	2.72
	12:128	28.01	2.34	29.00	2.42
	1:128	3.19	3.19	3.41	3.41
+2 Charge	4:128	11.58	2.90	15.60	3.90
	12:128	35.81	2.98	41.30	3.44

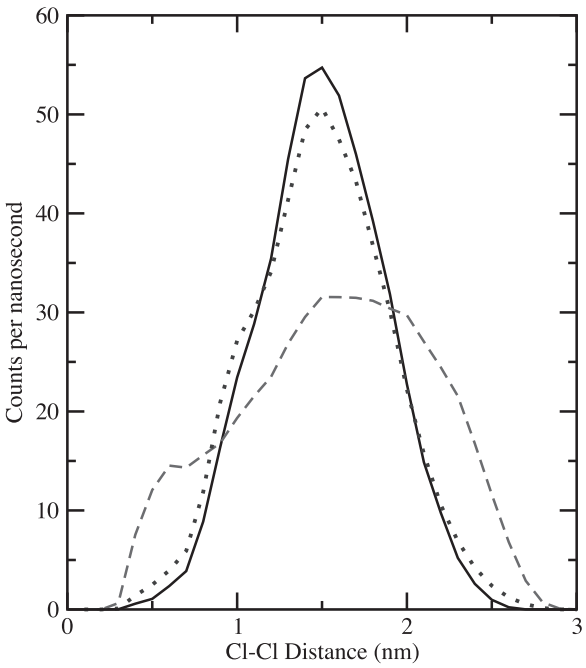

Fig. 9. Cl–Cl distance histogram of twelve +2 charged CHX during the first 10 ns at 323 K before insertion (dashed), for 10 ns after insertion (dotted), and the last 10 ns at 309K (solid).

CHX molecule makes an average of 2.5 hydrogen bonds, while the +2 CHX makes 3.5. As the concentration of CHX increases, the amount of hydrogen bonds decreases, possibly due to competition for hydrogen bond donors from the lipids.

The general conformation of the CHX molecule as being either compressed or expanded, was measured by tracing the distance between the two chlorine atoms of the chlorophenol rings located on the ends of the molecule. Initially while the CHX molecule was in water, a broad distribution of Cl-Cl distances was observed varying from 0.2 to 3.0 nm (Fig. 9). This corresponds to a wide range of changing conformations from it's compressed state to a extended state. After insertion into the membrane the distribution narrows significantly suggesting that there exists a more stable conformation. The distribution of distances is centred around ~1.5 nm, which is neither the most compressed state nor the most expanded state of the molecule but rather a "wedge" shape. Fig. 10 shows an example of this configuration. Not that the chlorine atoms generally point down or in the plane of the bilayer, but almost never point upwards towards the water.

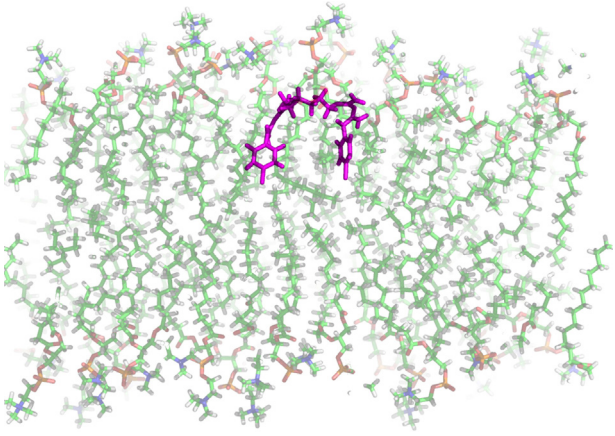

Fig. 10. Simulation snapshot of the neutral CHX molecule (solid purple) after insertion into DMPC at 323 K.

4. Discussion

The simulation's Stockholm-lipids parameters (Slipids) are refined based in large part on simulated liquid alkane density, and verified using experimentally determined membrane structural parameters provided by Kucerka et al. [33,1,2]. Our simulations of pure DMPC bilayers reproduce the published results without issue. Note that the double-layered distribution of water seen in Fig. 5 appears in every simulation, and is a consequence of the chosen parametrization of the lipids. Similar simulations in turn form the basis of the experimental analysis of the small angle scattering (X-ray and neutron combined) of Kucerka et al., where the double-layers can also be seen. There is little comment to be found in these papers on this second, more deeply penetrating layer of water; our data, and similar data from other neutron diffraction experiments do not find such water distributions.

The discrepancy could be a consequence of the fact that Kucerka et al. use dilute, small unilamellar vesicles versus our aligned, slightly dehydrated lamellar membrane stacks with approximately 5 water molecules per lipid. Another possibility is the fact that in Kucerka's model, the water is modelled as the absence of lipid; the molecular volume probability is kept at all points. It is difficult to asses this point, since the data fitting analysis of Kucerka et al. is likely over-parametrized, and no error estimation of the fitted parameters are provided. Indeed, less imposing water distributions can fit the data equally well [34]. Nevertheless, we believe the Slipids parameter set to be state-of-the-art, and the measured structural parameters of Kucerka et al. to be the most self-consistent and reasonable to date.

Whatever the case, even though the experiments do not agree on where the lipid–water interface lies, they both agree qualitatively that that is where the CHX molecule resides. The depth of CHX had little dependence on the concentration of the molecules used, rather it was more dependent on the charge. The neutral CHX were distributed around 0.8 nm from the bilayer center and were observed to spend time at the center at higher concentrations. The charged CHX models were seen further out of the membrane at 1.1 and 1.3 nm respectively and were not seen at the center of the membrane.

The more CHX we added to the DMPC membrane, the thinner it becomes, increasing the area per lipid accordingly. The charge of the CHX determined the degree of deformation of the membrane. The neutral model had a minimal effect to the change in area as well as the thickness and ordered the lipid chains. Both of the charged models had similar but more pronounced deformations to the area and thickness, however it lowered the chain order.

Initial placement of an membrane-active molecule into a simulation presents an interesting challenge. On the one hand, a membrane-protein system can be computationally large, and since simulation times are necessarily relatively short, they may not be long enough for whole body equilibration and rearrangement of the system so that the protein finds its appropriate place in the bilayer. In such cases, experimental information is required to set up the system properly [35,36]. For smaller molecules like CHX, one can hope for rapid diffusion to overcome this problem, unless there is some unforeseen energy barrier that traps the molecule in a metastable location.

Neither neutrality or charge prevents the molecule from seeking the same most energetically favourable position within the bilayer within a reasonable amount of time. However, an increase in the concentration of CHX increases the amount of intermolecular interactions and thus increases the amount of time needed for the

system to reach an equilibrium state. At a concentration of 12:128 CHX:DMPC the molecules had to be started close to the membrane to reduce the amount of time where the molecules interacted with one another in the water before finding their way into the membrane. Higher concentrations are not possible under these same time scales for this reason.

Remarkably our results confirm our experiments that a DMPC bilayer can accommodate a significant number of highly charged molecules without significant disruption to the underlying bilayer structure. This has two important consequences. First, +2 charged CHX is not a good candidate for umbrella sampling technique to determine the free energy profile in the bilayer. Any attempt to hold the location of a lone charged CHX deeper in the bilayer than its free energy location will severely distort the bilayer by opening a hole above it that will draw in water. This has been seen before in the case of arginine [37], and was the impetus for our brute-force methods here. Second, our results call into question the biological relevance of DMPC as a membrane mimic in studies of CHX. The remarkable capacity of DMPC to incorporate CHX is much higher than the minimum inhibitory concentration of the drug, which has been observed to be as low as 0.5 μg/ml for certain bacteria [38]. This corresponds to a CHX:lipid ratio of approximately 1:100 compared to our highest concentration of 12:128. We have demonstrated the rapid hydrophilic/phobic interface seeking ability of CHX, however DMPC must be more structurally robust than the components of bacterial, yeast, and viral membranes.

In conclusion, we have conducted a series of molecular dynamics simulations of chlorhexidine in DMPC. The Slipids force field serves as a state-of-the-art parameter set to reproduce many pure lipid bilayer properties very well, and serves as a basis of our simulations. Here we have seen for the first time how the Slipids DMPC can accommodate a high concentration of solute molecules, even +2 charged, with little change in structural integrity. This is in total agreement with our experience with experimental samples of the same concentration. However, for the case of the molecule chlorhexidine, which quickly seeks the hydrophilic/hydrophobic interface, the Slipids presents a water/lipid interface at a different location than was experimentally measured. This may be a consequence of the sample type, or the parameter set itself, and must be considered further.

Acknowledgements

This work wade possible by the facilities of the Shared Hierarchical Academic Research Computing Network (SHARCNET:www.sharcnet.ca) and Compute/Calcul Canada.

Appendix A. Supplementary Data

Supplementary data associated with this article can be found, in the online version, at http://dx.doi.org/10.1016/j.jmgm.2013.12.007.

References

[1] J.P.M. Jämbeck, A.P. Lyubartsev, Derivation and systematic validation of a refined all-atom force field for phosphatidylcholine lipids, The Journal of Physical Chemistry B 116 (10) (2012) 3164–3179.
[2] J.P.M. Jämbeck, A.P. Lyubartsev, Another piece of the membrane puzzle: extending slipids further, Journal of Chemical Theory and Computation 9 (2013) 774–784.
[3] N. Kucerka, J. Katsaras, J. Nagle, Comparing membrane simulations to scattering experiments: introducing the SIMtoEXP software, The Journal of membrane biology 235 (1) (2010) 43–50, research Support, Non-U.S. Gov't,Research Support, N.I.H., Extramural.
[4] I. Vorobyov, L. Li, T.W. Allen, Assessing atomistic and coarse-grained force fields for protein–lipid interactions: the formidable challenge of an ionizable side chain in a membrane, Journal of Physical Chemistry B 112 (2008) 9588–9602.
[5] R.K. Campbell, J. White, B.A. Saulie, Metformin: a new oral biguanide, Clinical Therapeutics 18 (3) (1996) 360–371.
[6] H. Uchiyama, A. Okamoto, K. Sato, T. Yamada, S. Murakami, S. Yoneda, Y. Kajita, T. Tegoshi, N. Arrizono, Quinine-resistant severe falciparum malaria effectively treated with atovaquone and proguanil hydrochloride combination therapy, Internal Medicine 43 (7) (2004) 624–627.
[7] L. Thomas, A. Russell, J.-Y. Maillard, Antimicrobial activity of chlorhexidine diacetate and benzalkonium chloride against *Pseudomonas aeruginosa* and its response to biocide residues, Journal of Applied Microbiology 98 (3) (2005) 533–543.
[8] A. Denys, T. Machlański, J. Bialek, S. Mrozicki, Relationships between chemical structure and antiviral activity of some biguanide derivatives., Zentralblatt Für Bakteriologie, Parasitenkunde, Infektionskrankheiten Und Hygiene. Erste Abteilung Originale. Reihe B: Hygiene, Präventive Medizin 164 (1–2) (1977) 85–89.
[9] J.M. Tanzer, A.M. Slee, B.A. Kamay, Structural requirements of guanide, biguanide, and bisbiguanide agents for antiplaque activity, Antimicrobial Agents and Chemotherapy 12 (6) (1977) 721–729.
[10] R.S. Blackburn, A. Harvey, L.L. Kettle, J.D. Payne, S.J. Russell, Sorption of poly(hexamethylenebiguanide) on cellulose: mechanism of binding and molecular recognition, Langmuir 22 (2006) 5636–5644.
[11] R.S. Blackburn, A. Harvey, L.L. Kettle, A.P. Manian, J.D. Payne, S.J. Russell, Sorption of chlorhexidine on cellulose: mechanism of binding and molecular recognition, Journal of Physical Chemistry B 111 (2007) 8775–8784.
[12] J. Yoo, Q. Cui, Does arginine remain protonated in the lipid membrane? Insights from microscopic pK_a calculations, Biophysical Journal: Biophysical Letters 94 (8) (2008) L61–L63.
[13] L. Li, I. Vorobyov, T.W. Allen, Potential of mean force and pKa profile calculation for a lipid membrane-exposed arginine side chain, Journal of Physical Chemistry B 112 (2008) 9574–9587.
[14] A. MacKerel Jr., C. Brooks III, L. Nilsson, B. Roux, Y. Won, M. Karplus, CHARMM: The Energy Function and Its Parameterization with an Overview of the Program, Vol. 1 of The Encyclopedia of Computational Chemistry, John Wiley & Sons, Chichester, 1998, pp. 271–277.
[15] B. Brooks, R. Bruccoleri, D. Olafson, D. States, S. Swaminathan, M. Karplus, CHARMM: a program for macromolecular energy, minimization, and dynamics calculations, Journal of Computational Chemistry 4 (1983) 187–217.
[16] B.R. Brooks, I.C.L. Brooks, J.A.D. Mackerell, L. Nilsson, R.J. Petrella, B. Roux, Y. Won, G. Archontis, C. Bartels, S. Boresch, A. Caflisch, L. Caves, Q. Cui, A.R. Dinner, M. Feig, S. Fischer, J. Gao, M. Hodoscek, W. Im, K. Kuczera, T. Lazaridis, J. Ma, V. Ovchinnikov, E. Paci, R.W. Pastor, C.B. Post, J.Z. Pu, M. Schaefer, B. Tidor, R.M. Venable, H.L. Woodcock, X. Wu, W. Yang, D.M. York, M. Karplus, CHARMM. The biomolecular simulation program, Journal of Computational Chemistry 30 (10 (Sp. Iss. SI)) (2009) 1545–1614.
[17] W.F. van Gunsteren, S.R. Billeter, A.A. Eising, P.H. Hünenberger, P. Krüger, A.E. Mark, W.R.P. Scott, I.G. Tironi, Biomolecular Simulation: The GROMOS96 Manual and User Guide, Hochschulverlag AG an der ETH Zürich, Zürich, Switzerland, 1996.
[18] M.J. Frisch, G.W. Trucks, H.B. Schlegel, G.E. Scuseria, M.A. Robb, J.R. Cheeseman, G. Scalmani, V. Barone, B. Mennucci, G.A. Petersson, H. Nakatsuji, M. Caricato, X. Li, H.P. Hratchian, A.F. Izmaylov, J. Bloino, G. Zheng, J.L. Sonnenberg, M. Hada, M. Ehara, K. Toyota, R. Fukuda, J. Hasegawa, M. Ishida, T. Nakajima, Y. Honda, O. Kitao, H. Nakai, T. Vreven, J.J.A. Montgomery, J.E. Peralta, F. Ogliaro, M. Bearpark, J.J. Heyd, E. Brothers, K.N. Kudin, V.N. Staroverov, R. Kobayashi, J. Normand, K. Raghavachari, A. Rendell, J.C. Burant, S.S. Iyengar, J. Tomasi, M. Cossi, N. Rega, J.M. Millam, M. Klene, J.E. Knox, J.B. Cross, V. Bakken, C. Adamo, J. Jaramillo, R. Gomperts, R.E. Stratmann, O. Yazyev, A.J. Austin, R. Cammi, C. Pomelli, J.W. Ochterski, R.L. Martin, K. Morokuma, V.G. Zakrzewski, G.A. Voth, P. Salvador, J.J. Dannenberg, S. Dapprich, A.D. Daniels, Ö. Farkas, J.B. Foresman, J.V. Ortiz, J. Cioslowski, D.J. Fox, Gaussian 09 Revision B.01, Gaussian Inc., Wallingford, CT, 2009.
[19] I. Komljenović, D. Marquardt, T.A. Harroun, E. Sternin, Location of chlorhexidine in DMPC model membranes: a neutron diffraction study, Chemistry and Physics of Lipids 163 (2010) 480–487.
[20] L. Adane, P.V. Bharatam, Tautomeric preferences and electron delocalization in biurets, thiobiurets, and dithiobiurets: an ab initio study, International Journal of Quantum Chemistry 108 (2008).
[21] P.V. Bharatam, D.S. Patel, P. Iqbal, Pharmacophoric features of biguanide derivatives: an electronic and structural analysis, Journal of Medicinal Chemistry 48 (2005) 7615–7622.
[22] Z.B. Maksić, B. Kovačević, Absolute proton affinity of some polyguanides, Journal of Organic Chemistry 65 (2000) 3303–3309.
[23] R. Guha, M.T. Howard, G.R. Hutchison, P. Murray-Rust, H. Rzepa, C. Steinbeck, J.K. Wegner, E.L. Willighagen, The blue obelisk-interoperability in chemical informatics, Journal of Chemical Information and Modeling 46 (2006) 991–998.
[24] N.M. O'Boyle, M. Banck, C.A. James, C. Morley, T. Vandermeersch, G.R. Hutchison, v2.2.3, 2011.
[25] M.D. Hanwell, D.E. Curtis, D.C. Lonie, T. Vandermeersch, E. Zurek, G.R. Hutchison, Avogadro: an advanced semantic chemical editor, visualization, and analysis platform, v1.0.3, 2012.
[26] M. Valiev, E. Bylaska, N. Govind, K. Kowalski, T. Straatsma, H.V. Dam, D. Wang, J. Nieplocha, E. Apra, T. Windus, W. de Jong, NWChem: a comprehensive and scalable open-source solution for large scale molecular simulations, Computer Physics Communications 181 (9) (2010) 1477–1489.

[27] S. Jo, T. Kim, V.G. Iyer, W. Im, CHARMM-GUI: a web-based graphical user interface for CHARMM, Journal of Computational Chemistry 29 (11) (2008) 1859–1865.
[28] A. Kukol, Lipid models for united-atom molecular dynamics simulations of proteins, Journal of Chemical Theory and Computation 5 (2009) 615–626.
[29] D. Poger, A.E. Mark, On the validation of molecular dynamics simulations of saturated and cis-monounsaturated phosphatidylcholine lipid bilayers: a comparison with experiment, Journal of Chemical Theory and Computation 6 (2010) 325–336.
[30] B. Hess, C. Kutzner, D. van der Spoel, E. Lindahl, GROMACS 4: algorithms for highly efficient, load-balanced, and scalable molecular simulation, Journal of Chemical Theory and Computation 4 (3) (2008) 435–447.
[31] S.K. Schiferl, D.C. Wallace, Statistical errors in molecular dynamics averages, Journal of Chemical Physics 83 (10) (1995) 5203–5209.
[32] N. Kučerka, J.F. Nagle, J.N. Sachs, S.E. Feller, J. Pencer, A. Jackson, J. Katsaras, Lipid bilayer structure determined by the simultaneous analysis of neutron and X-ray scattering data, Biophysical Journal 95 (2008) 2356–2367.
[33] N. Kučerka, M.-P. Nieh, J. Katsaras, Fluid phase lipid areas and bilayer thicknesses of commonly used phosphatidylcholines as a function of temperature, Biochimica et Biophysica Acta 1808 (2011) 2761–2771.
[34] N. Kučerka, J.F. Nagle, S.E. Feller, P. Balgavý, Models to analyze small-angle neutron scattering from unilamellar lipid vesicles, Physical Review E 051903 (2004) 1–9.
[35] F. Basyn, B. Spies, O. Bouffioux, A. Thomas, R. Brasseur, Insertion of X-ray structures of proteins in membranes, Journal of Molecular Graphics and Modelling 22 (2003) 11–21.
[36] K. Balali-Mood, T.A. Harroun, J.P. Bradshaw, Membrane-bound ARF1 peptide: interpretation of neutron diffraction data by molecular dynamics simulation methods, Molecular Membrane Biology 22 (5) (2005) 379–388.
[37] J.L. MacCallum, W.D. Bennett, D.P. Tieleman, Transfer of arginine into lipid bilayers is nonadditive, Biophysical Journal 101 (1) (2011)110–117.
[38] A. Fraise, J. Maillard, S. Sattar, Russell, Hugo and Ayliffe's Principles and Practice of Disinfection, Preservation and Sterilization [electronic resource], Wiley, Hoboken, 2012.